Revista de Metalurgia
April-June 2021, 57 (2), e192
ISSN-L: 0034-8570
https://doi.org/10.3989/revmetalm.192

Mechanical and wear characteristics of duplex stainless steels using Taguchi's grey relational analysis

C. Rajkumar, J. Udaya Prakash, Sachin Salunkhe*, S. Jayavelu

Department of Mechanical Engineering, Vel Tech Rangarajan Dr. Sagunthala R&D Institute of Science and Technology, Avadi High Rd, Vel Nagar, Chennai, Tamil Nadu 600062, India

(*Corresponding author: drsalunkhesachin@veltech.edu.in)

Submitted: 6 August 2020; Accepted: 4 February 2021; Available On-line: 29 June 2021

ABSTRACT: Sintered components fabricated from Duplex Stainless Steels (DSS) are suitable for many applications. Duplex Stainless Steels are the combination of ferritic and austenitic stainless steels employed in different industries owing to their combined mechanical and corrosion properties. The usage of DSS is growing up year by year in automobile industries and offshore industries. In this paper, two-phase structure steels fabricated by powder metallurgy route are presented. DSS A and DSS B are the two compositions made by prealloyed powders (310L and 430L) along with ferrite and austenite stabilisers such as chromium, molybdenum, and nickel. The powders were blended in a pot mill for 12 h. Sintering of powder preforms was carried out at 1350 ºC in partial vacuum and hydrogen atmospheres, respectively. Sintered compacts were subjected to forge operation at 1150 ºC and quenched in water. XRD analysis of sintered and forged DSS confirms the absence of intermetallics. The mechanical and wear behavior of DSS were analyzed using Taguchi's Grey Relational Analysis. DSS B in forged condition subjected to 20N loading conditions under hydrogen atmosphere exhibited COF of 0.53.

KEYWORDS: Duplex stainless steels; Forging; Grey relational analysis; Partial vacuum; Powder Metallurgy; Wear

Citation/Citar como: Rajkumar, C.; Udaya Prakash, J.; Salunkhe, S.; Jayavelu, S. (2021). "Mechanical and wear characteristics of duplex stainless steels using Taguchi's grey relational analysis". *Rev. Metal.* 57(2): e192. https://doi.org/10.3989/revmetalm.192

RESUMEN: *Propiedades mecánicas y desgaste de aceros inoxidables dúplex utilizando el método de Taguchi de análisis de imagen.* Los componentes sinterizados fabricados con aceros inoxidables dúplex (DSS) son adecuados para aplicaciones muy diversas. Los aceros DSS son una combinación de aceros inoxidables ferríticos y austeníticos, y son ampliamente utilizados en diferentes industrias debido a sus buenas propiedades mecánicas y de resistencia a la corrosión. El uso de DSS está creciendo año tras año en la industria del automóvil y en las industrias offshore. En el presente trabajo se estudian dos aceros, DSS A y DSS B, con estructura bifásica obtenidos por vía pulvimetalúrgica. Se utilizaron dos composiciones hechas con polvos prealeados (AISI 310L y AISI 430L) junto con estabilizadores de ferrita y austenita como cromo, molibdeno y níquel. Los polvos se mezclaron en un molino durante 12 h. La sinterización de las preformas en polvo se realizó a 1350 ºC en vacío parcial y en atmósfera de hidrógeno, respectivamente. Los compactos sinterizados se sometieron a operación de forjado a 1150 ºC y se enfriaron en agua. El análisis XRD del DSS sinterizado y forjado confirmó la ausencia de intermetálicos. El comportamiento mecánico y desgaste de DSS se analizó mediante el análisis relacional de grises del método de Taguchi. El DSS B en estado forjado sometido a condiciones de carga de 20 N bajo atmósfera de hidrógeno mostró un COF de 0,53.

PALABRAS CLAVE: Aceros inoxidables dúplex; Análisis relacional de grises; Desgaste; Forjar; Metalurgia de polvos; Vacío parcial

ORCID ID: C. Rajkumar (https://orcid.org/0000-0002-4316-2566); J. Udaya Prakash (https://orcid.org/0000-0001-9229-5499); Sachin Salunkhe (https://orcid.org/0000-0001-6542-2050); S. Jayavelu (https://orcid.org/0000-0001-6950-1979)

1. INTRODUCTION

Duplex Stainless Steels (DSS) are those, which have approximately equal proportions of austenite and ferrite microstructure. DSS possess more strength than austenitic stainless steels, and they have more excellent toughness than ferritic stainless steels, which are more resistant to several corrosive types in various corrosive environments (Olsson and Growth, 1994; Badji *et al.*, 2008; Gideon *et al.*, 2008). DSS is widely used in food processing plants, automobile applications, petrochemical plants, marine water desalination plants, where high mechanical strength and corrosion resistance are critical (Campos *et al.*, 2003; Olsson and Sniss, 2007). The methodology for the fabrication of DSS is casting and powder metallurgy. Further fabrication of DSS, is a complex process due to its element's contents. The elements such as chromium, nickel, and nitrogen affect the formation of intermetallics of DSS. (Marcu Puscas *et al.*, 2001; Haghdadi *et al.*, 2018). DSS fabricated through powder metallurgy attracts many industrial applications (Raja Annamalai *et al.*, 2015). Various methods are usually used in the current technology to produce DSS through powder metallurgy. One such method is using 316L (austenitic) or 410L (ferritic) pre-alloyed base powders with alloying elemental powders to obtain DSS. DSS obtained by 410L (ferritic) achieved good mechanical properties (Brytan *et al.*, 2011).

Various researchers from around the world are working on the mechanical and wear properties of DSS. They stated that the wear performance of Super DSS was increased through escalating sigma amount fraction in ferrite/austenite matrix (Fargas *et al.*, 2013). The wear properties of nitrogen sintered DSS are better than argon sintered DSS due to more lamellar constituents with ferrite matrix (Mariappen *et al.*, 2015). Mestra *et al.* (2010) analyzed the wear features of DSS. They reported that the wear rate relies upon sliding distance and velocity. The wear mechanisms observed are plowing, microcracking, and micro-cutting. The tensile strength or yield strength of the DSS is increased when the sigma phases formed in the DSS are within the range from 700 °C to 850 °C (Pohl *et al.*, 2007). The mechanical properties of DSS 25Cr-7Ni and 22Cr-5Ni (wt percent) aged at 325 °C depend on phase separation (Xu *et al.*, 2019). The characteristics of grain and phase influence the mechanical properties of the DSS. The hardness of DSS is 1.5 times higher than that of austenitic and ferritic stainless steels. The latest study reveals (Okayasu and Ishida, 2019) the analysis of the parametric effect of speed, feed, and depth of cut on performance characteristics (i.e.) feed, surface roughness, metal removal rate during wet turning of super duplex stainless steels UNS S32760 using nano-coated MEGACOAT carbide inserts. Surface roughness and feed are minimized to achieve maximum performance, and the metal removal rate is maximized using Taguchi-grey relational analysis (Dinde and Dhende, 2021). From the available literature, it is found that very few are available for analysis of Powder metallurgy DSS mechanical and wear behavior using Taguchi's Gray Relational Analysis. Therefore, this research aims to develop Powder Metallurgy DSS using 310L and 430L powders, together with the addition of chromium, nickel, and molybdenum, and to analyze the mechanical and wear behavior using the Gray Relational Analysis.

2. MATERIALS AND METHODS

The materials used in this investigation are 310L austenitic stainless steel and 430L ferric stainless-steel powders, together with elemental chromium, molybdenum, nickel, and copper. For the samples' preparation, there are two DSS, namely A and B, made up of 310L and 430L pre-alloyed powders. The following are the compositions of two DSS A and B:

(DSS A) - (50%310L+50%430L) by wt
(DSS B) - (45%310L+45%430L+4%Ni+5%Cr+1% Mo) by wt

The chemical constituents of DSS, their chromium, and nickel equivalent numbers are shown in Table 1. The powder mixtures were compacted at 550 MPa in the Universal Testing Machine. The green compact dimensions are 10 mm in height and 30 mm in diameter. Further, green compacts were sintered in the hot press of the vacuum furnace. The sintering operation took place at 1350 °C for 2 h. The sintering operation was performed in partial vacuum and hydrogen atmospheres. The sintered samples were stored in an electrical muffle furnace at a temperature of 1150 °C for 2 h, and the samples were forged at that temperature using a 100-ton friction screw press.

Micro tensile samples as per ASTM E8 were machined from sintered stainless steels. Digital Tensome-

Table 1. Chemical constituents of DSS

Composition	Elemental Concentration (%wt)									
	Ni	Cr	C	Si	Mn	Mo	Fe	Ni_{eq}	Cr_{eq}	PREN
DSS A	5	20.3	0.02	0.75	1.05	0.15	Bal.	6.1	21.57	20.53
DSS B	8.5	23.27	0.018	0.67	0.945	1.13	Bal.	9.51	25.41	27.01

ter was used to perform a micro-tensile test. Rockwell Hardness Testing Machine (TRS model) was used to perform hardness testing on all sintered duplex stainless steels. In this investigation, diamond 1/16 "indenter and 100 kgf significant load was used. The obtained values of hardness are the mean of six penetrations at the various places of the specimens indicated. The pin on the disc wear testing machine is shown in Fig 1.

Pin-on-disc is used to determine the wear characteristics of the PM duplex stainless steel performs. The variables affecting friction and wear are the sliding velocity, the sliding distance, and the load. The size of the pin is 3 mm in radius and 34 mm in length. Duplex stainless steel was used as a pin material, a counter disk with a diameter of 65 mm and a thickness of 10 mm was manufactured using high-carbon chromium steel (die steel). The disk and pin were washed through acetone to confirm that the wear tests were carried out under dry sliding conditions. The measurement of weight loss was used to calculate the rate of wear. Tests were conducted at 20N and 30N, respectively. The sliding speed and the sliding distance were kept constant at 2 $m \cdot s^{-1}$ and 750 m. The test was performed at room temperature.

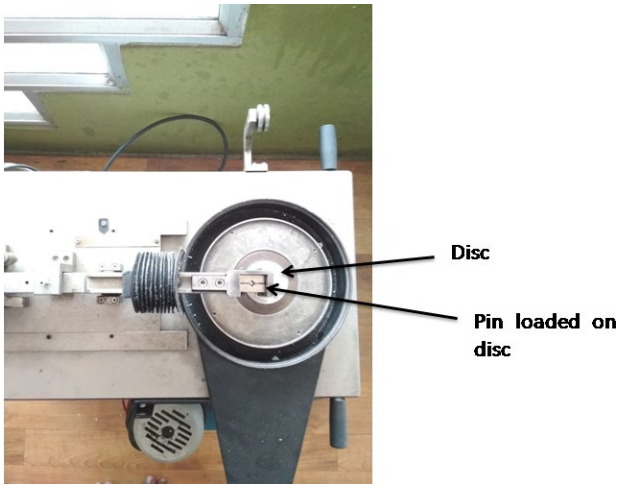

Figure 1. Pin on Wear Testing Machine.

3. RESULTS AND DISCUSSION

3.1. Microstructure study of sintered DSS

DSS is well polished and etched with Berahaa solution during the micro-structural inspection. The microstructures of DSS sintered in a partial vacuum with a bi-phase structure with varied amounts of ferrite and austenite are shown in Fig. 2.

The differences in ferrite content of the DSS depend on the chemical composition and thermal treatment. The optical microstructures of hydrogen sintered DSS A and B are shown in Fig. 3. Hydrogen sintered DSS microstructures reveal a duplex

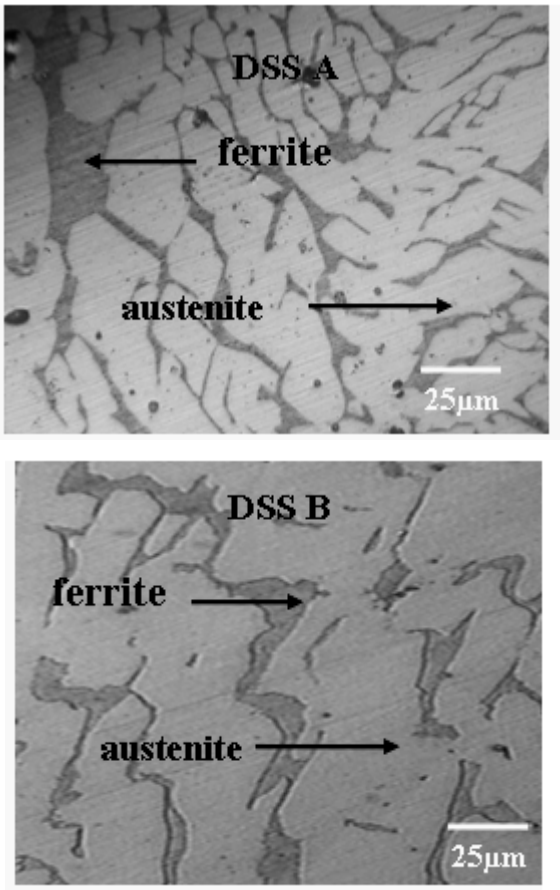

Figure 2. Microstructures of DSS Sintered in Partial Vacuum.

structure of ferrite and austenite with varying percentages of volume.

3.2. Microstructure study of forged DSS

The microstructure of the forged DSS sintered in partial vacuum and hydrogen is shown in Fig. 4. Figure 4a shows DSS A's microstructure, which consists of part acicular and angular types of ferritic grains along with the austenitic phase. Besides, Fig. 4b shows the elongated and ferrite grains of different sizes and orientations. A similar structure was also found for hydrogen sintered steels (DSS A and B). DSS B extended ferrite nature is because of the ferrite grain proliferates during sintering the composition of DSS B compared to DSS A. The faster growth of ferrite grains and elongated cells has been affected by higher chromium/nickel levels of DSS B composition (23Cr-8.5 Ni). The lower nickel and chromium content of the DSS A composition (20.3Cr-5Ni) decreased the ferrite rate. In addition to this bi-phase structure, there is no evidence of undesirable precipitates, namely sigma, chi phases, or secondary austenitic structure formation.

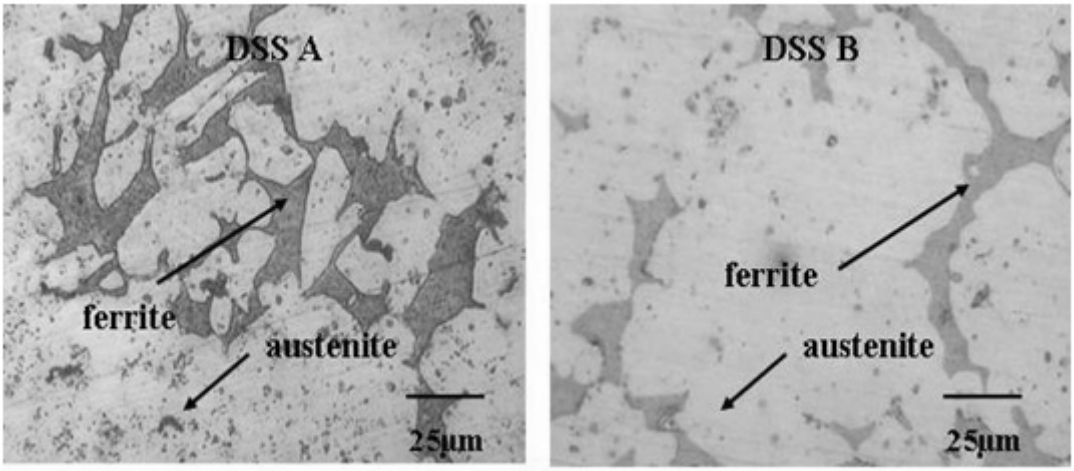

Figure 3. Microstructures of DSS Sintered in Hydrogen Atmosphere.

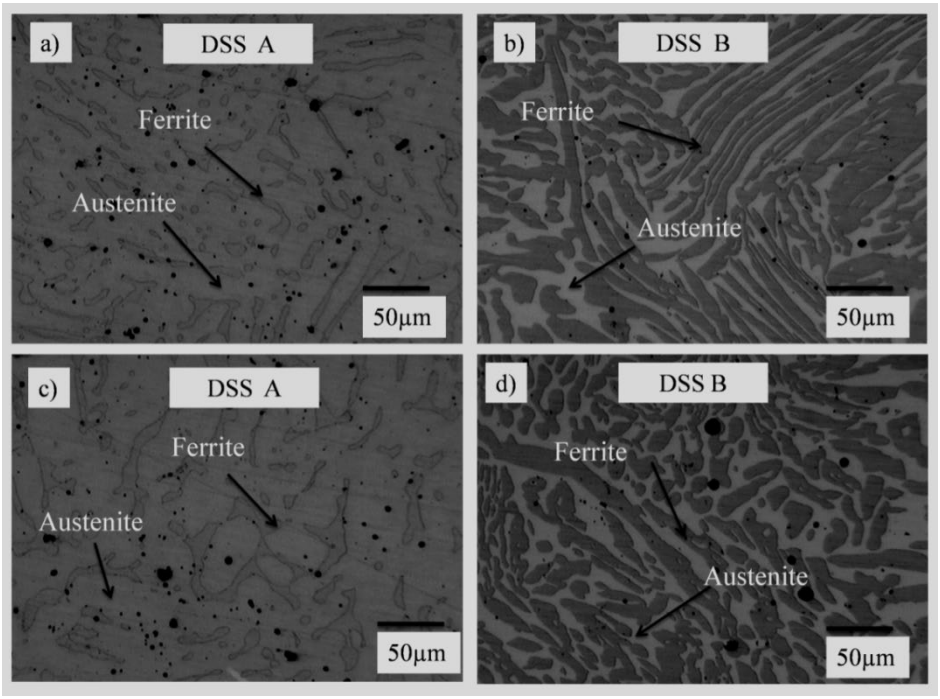

Figure 4. Microstructure of Forged DSS Sintered in (a) and (b), Partial Vacuum (c) and (d) Hydrogen Atmosphere.

3.3. XRD Analysis of sintered DSS

The XRD patterns of DSS sintered in partial vacuum and hydrogen are shown in Fig. 5 and Fig. 6. From these XRD patterns, it is clear that the DSS sintered in partial vacuum and hydrogen atmosphere do not show any sigma peaks and free form intermetallics. The variation in the intensities of austenite and ferrite peaks depends on the chemical composition of the DSS.

3.4. XRD analysis of forged DSS

The sintered DSS were held in a muffle furnace at the temperature of 1050 °C for 2 h, and the samples were forged at that temperature using 100 ton friction screw press. The purpose of forging is to enhance the density as well as mechanical properties. The XRD patterns forged DSS in a partial vacuum and hydrogen atmosphere are shown in Fig. 7 and Fig. 8. After forging, the samples were water quenched. The XRD patterns of forged DSS also reveal the absence of intermetallics. XRD patterns of DSS forged in partial vacuum shows more ferrite peaks compared to DSS forged in hydrogen atmosphere.

3.5. Mechanical properties – Grey relational analysis

Grey relational analysis (GRA) is combined with Taguchi's method for optimizing multiple perfor-

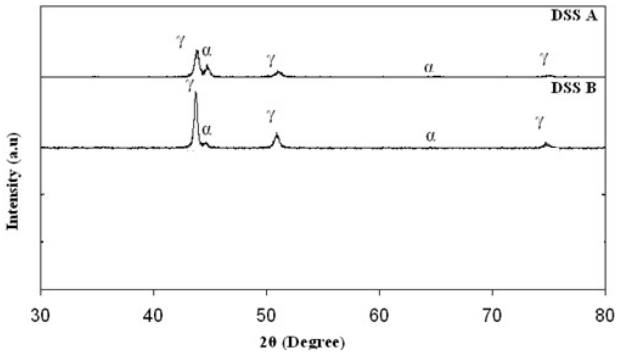

Figure 5. XRD Patterns of DSS Sintered in Partial Vacuum.

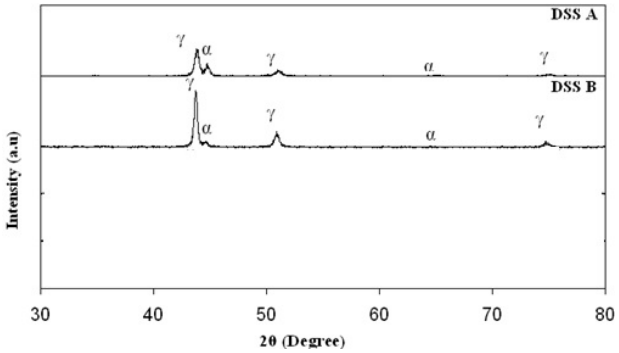

Figure 6. XRD Patterns of DSS Sintered in Hydrogen Atmosphere.

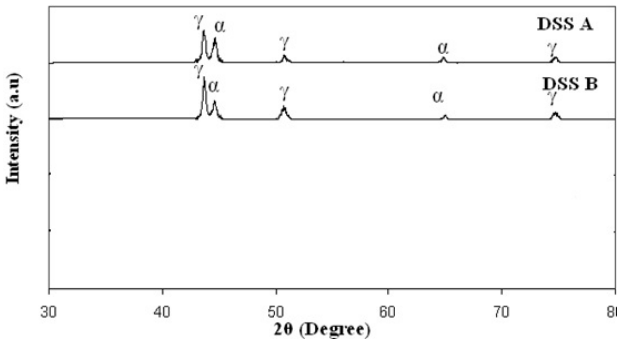

Figure 7. XRD Patterns of Forged DSS Sintered in Partial Vacuum.

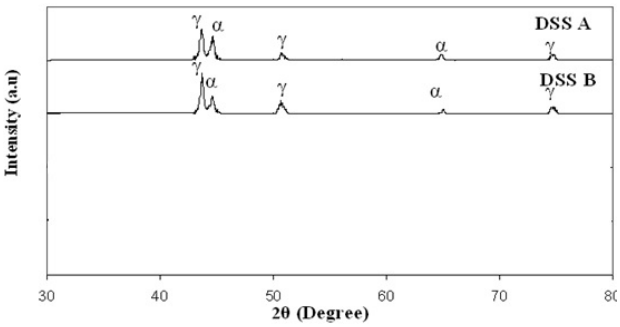

Figure 8. XRD Patterns of Forged DSS Sintered in Hydrogen Atmosphere.

mance characteristics. The process parameters and their levels are tabulated in Table 2. The results of the investigation and GRG are shown in Table 3. The GRG was determined using the gray relational analysis of each variable at various levels from experimental data.

Figure 9 shows the response graphs for means. The response graphs are used to evaluate the parametric effects on response characteristics. The GRG data was analyzed to determine important variables and evaluate their effects on response characteristics.

Table 4 shows the response table for means. The response table shows the average of each response characteristics (GRG) data for each factor level. The response table reveals that condition is the main parameter affecting the mechanical properties, followed by atmosphere and material. ANOVA Table 5 shows that condition is the main parameter 47.45% affecting the means of mechanical properties.

3.5.1. Confirmation experiment for predicted means

Table 2. Process Parameters and their levels

Level	Material	Condition	Atmosphere	Load (N)
1	DSS A	Sintered	Hydrogen	20
2	DSS B	Forged	Partial Vacuum	30

By evaluating response graphs and mean tables, the optimal conditions for process variables are calculated using mean response characteristics. The optimum process parameters for predicted means and experimental values are given in Table 6. The optimum parameters are used for conducting the confirmation experiment and for predicting GRG. The predicted GRG is 0.941, and the experimental GRG is 0.966. The error is 2.5%, so the optimization technique holds good.

3.6. Grey relational analysis – Wear

The results of the investigation of wear and GRG are shown in Table 7. From experimental data using the Gray Relational Analysis, GRG

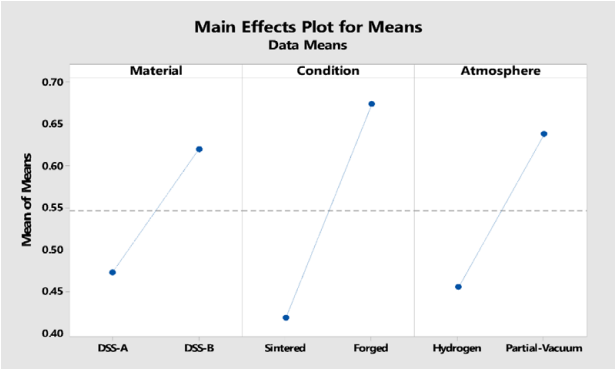

Figure 9. Response Graphs for GRG.

Table 3. Experimental Results of Mechanical Properties

S. No.	Material	Condition	Atmosphere	Density (g/cc)	Hardness (HRA)	Ultimate Stength (MPa)	Percentage Elongation	GRG	Rank
1	DSS-A	Sintered	H.P*	7.41	58	580	7.57	0.333	8
2	DSS-A	Sintered	Vacuum	7.57	60	637	12	0.432	6
3	DSS-A	Forged	H.P*	7.73	64	613	8.17	0.497	5
4	DSS-A	Forged	Vacuum	7.79	62	650	15	0.628	2
5	DSS-B	Sintered	H.P*	7.47	60	640	9.02	0.386	7
6	DSS-B	Sintered	Vacuum	7.61	65	658	14	0.523	4
7	DSS-B	Forged	H.P*	7.73	67	695	10.05	0.601	3
8	DSS-B	Forged	Vacuum	7.76	70	760	18	0.966	1

*Hydrogen-Partial

Table 4. Response Table for Means

Level	Material	Condition	Atmosphere
1	0.4724	0.4184	0.4541
2	0.619	0.673	0.6372
Delta	0.1466	0.2546	0.1831
Rank	3	1	2

for each variable were calculated at different levels.

Figure 10 shows the response graphs for means. The response graphs are used to evaluate the parametric effects on the response characteristics. Variance analysis is conducted with GRG data to determine the relevant variables and to measure their effects on response characteristics.

Table 8 shows the response table for means. The response table shows the average of each response characteristics (GRG) data for each factor level. The response table reveals that condition is the main parameter affecting the mechanical properties. ANOVA Table 9 reveals that the condition is the main parameter, 19.62% affecting the means of wear properties.

Table 6. Optimum Process Parameters for Predicted GRG

Material	Condition	Atmosphere	Predicted GRG	Experimental GRG
DSS-B	Forged	Partial Vacuum	0.941	0.966

3.6.1. Confirmation experiment for predicted means

Response graphs and means tables provide the best setting for process variables in terms of the mean response characteristics. For conduction of the confirmative experiment and estimation of GRG, the optimum parameters are used. Table 10 shows the optimum process parameters for predicted processes and experimental values. It is 0.729 for the predicted GRG and 0.926 for the experimental GRG. The failure is 19.7%.

3.6.2. SEM analysis of DSS worn samples

The SEM images of forged DSS samples sintered in a Hydrogen atmosphere are given in Fig. 11. Forged DSS A of SEM image reveals that it consists

Table 5. ANOVA for Means

Source	DF	Seq SS	Adj MS	F	P	Contribution %
Material	1	0.042998	0.042998	9.09	0.204	15.73
Condition	1	0.129668	0.129668	27.42	0.12	47.45
Atmosphere	1	0.06707	0.06707	14.18	0.165	24.54
Material*Condition	1	0.011063	0.011063	2.34	0.369	4.05
Material*Atmosphere	1	0.009282	0.009282	1.96	0.395	3.40
Condition*Atmosphere	1	0.008483	0.008483	1.79	0.408	3.10
Residual Error	1	0.004729	0.004729	9.09	-	1.73
Total	7	0.273292	-		-	100.00

Table 7. Experimental Results of Wear Properties

Exp No.	Load (N)	Material	Condition	Atmosphere	Wear Rate ($mm^3 \cdot m^{-1}$)	SWR ($mm^3 \cdot Nm^{-1}$)	COF	GRG	Rank
1	20	DSS-A	Sintered	Hydrogen	0.044	0.0022	0.522	0.653	6
2	20	DSS-A	Sintered	Partial-Vacuum	0.052	0.0026	0.602	0.443	14
3	20	DSS-A	Forged	Hydrogen	0.065	0.0033	0.565	0.447	13
4	20	DSS-A	Forged	Partial-Vacuum	0.016	0.0008	0.598	0.752	3
5	20	DSS-B	Sintered	Hydrogen	0.037	0.0018	0.548	0.611	7
6	20	DSS-B	Sintered	Partial-Vacuum	0.043	0.0021	0.62	0.471	11
7	20	DSS-B	Forged	Hydrogen	0.040	0.0020	0.525	0.663	5
8	20	DSS-B	Forged	Partial-Vacuum	0.014	0.0007	0.53	0.926	1
9	30	DSS-A	Sintered	Hydrogen	0.051	0.0017	0.56	0.551	9
10	30	DSS-A	Sintered	Partial-Vacuum	0.061	0.0020	0.633	0.426	15
11	30	DSS-A	Forged	Hydrogen	0.076	0.0025	0.59	0.421	16
12	30	DSS-A	Forged	Partial-Vacuum	0.041	0.0014	0.636	0.512	10
13	30	DSS-B	Sintered	Hydrogen	0.042	0.0014	0.575	0.572	8
14	30	DSS-B	Sintered	Partial-Vacuum	0.048	0.0016	0.669	0.457	12
15	30	DSS-B	Forged	Hydrogen	0.014	0.0005	0.562	0.883	2
16	30	DSS-B	Forged	Partial-Vacuum	0.030	0.0010	0.568	0.67	4

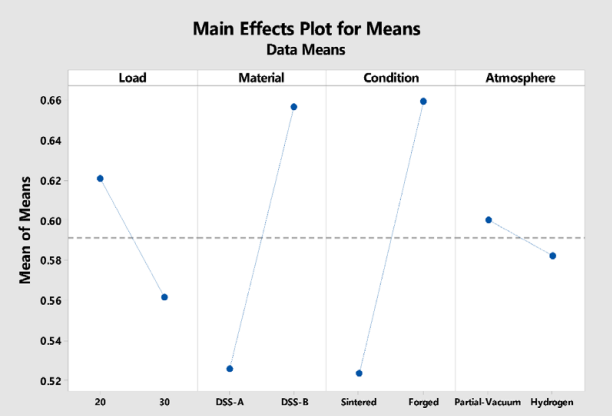

Figure10. Response Graphs for GRG (Wear Properties).

of more debris. The mechanism involved in worn-out wear surface is permanent deformation. Similarly, forged DSS B in hydrogen atmosphere consists of very small tiny pores.

The SEM images of forged DSS samples sintered in a Partial vacuum atmosphere are given in Fig. 12. The mechanism associated with the worn-out wear surface is due to plastic deformation. Both forged samples DSS A and B in partial vacuum atmosphere do not reveal any pores or ploughs, or debris.

4. CONCLUSIONS

The DSS A and B mechanical and wear experiments were conducted and analyzed with Grey Relational Analysis's aid. From the results of DSS A and B, the following primary observations were made:

Table 8. Response Table for GRG

Level	Load	Material	Condition	Atmosphere
1	0.6208	0.5256	0.523	0.6001
2	0.5615	0.6566	0.6593	0.5821
Delta	0.0593	0.131	0.1362	0.018
Rank	3	2	1	4

DSS B in forged condition subjected to 20N loading conditions under partial vacuum atmosphere exhibited SWR of 0.0007mm^3/Nm.

The statistical findings of the experiments were well aligned with the surface plots achieved. The model of wear intensity is statistically verified with ANOVA with a strong multi-coefficient correlation.

DSS B in forged condition subjected to 20N loading conditions under partial vacuum atmosphere exhibited COF of 0.53.

The model established is more suitable for automotive and offshore industries and inexperienced consumers to reach the lowest wear rate without realistic experiments.

REFERENCES

Badji, R., Bouabdallah, M., Bacroix, B., Kahloun, C., Belkessa, B., Maza, H. (2008). Phase transformation and mechanical behavior in annealed 2205 duplex stainless steel welds. *Mater. Charact.* 59 (4), 447-453. https://doi.org/10.1016/j.matchar.2007.03.004.

Table 9. ANOVA for GRG

Source	DF	Seq SS	Adj MS	F	P	Contribution %
Load	1	0.014042	0.01404	1.13	0.336	3.710868336
Material	1	0.068644	0.06864	5.53	0.065	18.14049609
Condition	1	0.074256	0.07426	5.98	0.058	19.62357493
Atmosphere	1	0.001296	0.0013	0.1	0.76	0.342492904
Load* Material	1	0.005476	0.00548	0.44	0.536	1.447138229
Load* Condition	1	0.001056	0.00106	0.09	0.782	0.279068292
Load* Atmosphere	1	0.021025	0.02103	1.69	0.25	5.556260273
Material* Condition	1	0.059049	0.05905	4.76	0.081	15.60483296
Material* Atmosphere	1	0.004422	0.00442	0.36	0.577	1.168598475
Condition* Atmosphere	1	0.067081	0.06708	5.41	0.068	17.7274433
Residual Error	5	0.062054	0.01241			16.39896195
Total	15	0.378402				100

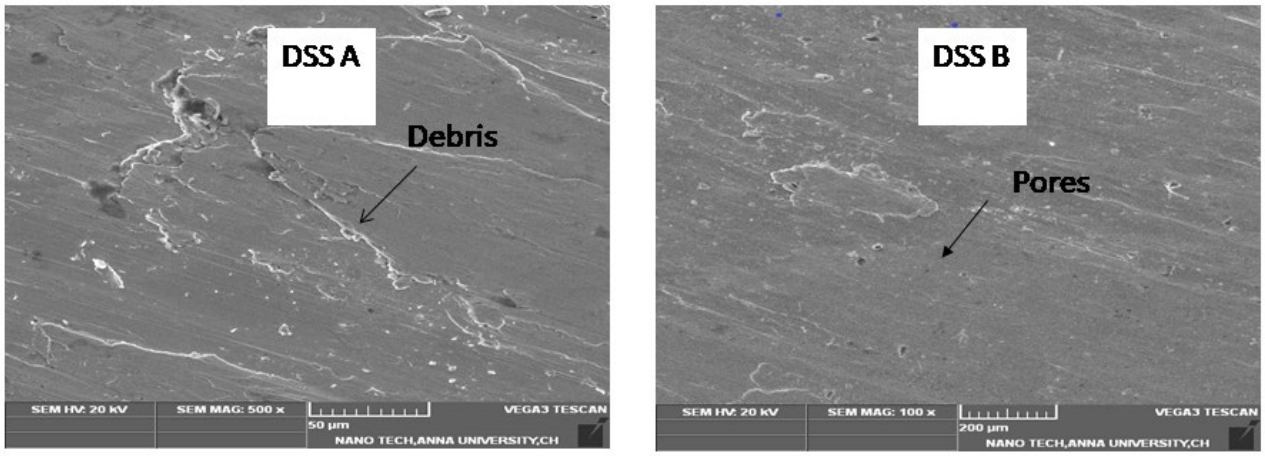

Figure 11. SEM Images of Forged DSS A and DSS B in Hydrogen Atmosphere.

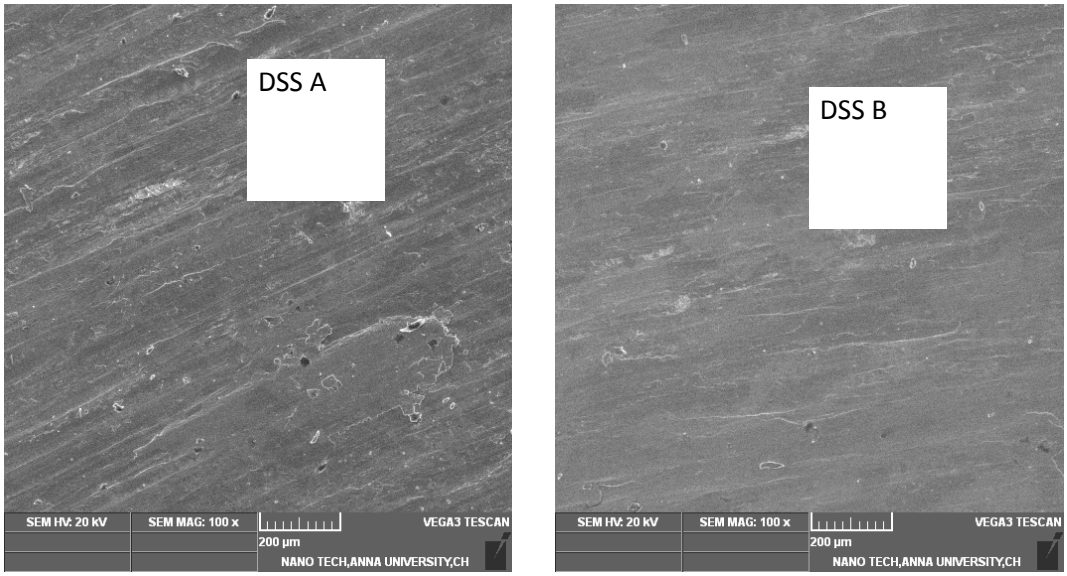

Figure 12. SEM Images of Forged DSS A and DSS B in Partial Vacuum Atmosphere.

Table 10. Optimum Process Parameters

Load (N)	Material	Condition	Atmosphere	Predicted GRG	Experimental GRG
20	DSS-B	Forged	Partial Vacuum	0.729	0.926

Brytan, Z., Grande, M.A., Rosso, M., Bidulský, R., Dobrzański, L.A. (2011). Stainless steels sintered form the mixture of prealloyed stainless steel and alloyin gelement powders. *Mater. Sci. Forum* 672, 165-170. https://doi.org/10.4028/www.scientific.net/MSF.672.165.

Campos, M., Bautista, A., Cáceres, D., Abenojar, J., Torralba, J.M. (2003). Study of the interfaces between austenite and ferrite grains in P/M duplex stainless steels. *J. Eur. Ceram. Soc.* 23 (15), 2813-2819. https://doi.org/10.1016/S0955-2219(03)00293-0.

Dinde, G., Dhende, G.S. (2021). *Multi-response Optimization of Process Parameters During Wet Turning of Super Duplex Stainless Steel UNS S32760 Using Taguchi-Grey Relational Analysis*. In *Optimization Methods in Engineering.* Springer, Singapore, pp. 417-428. https://doi.org/10.1007/978-981-15-4550-4.

Fargas, G., Mestra, A., Mateo, A. (2013). Effect of sigma phase on the wear behavior of a super duplex stainless steel. *Wear* 303 (1-2), 584-590. https://doi.org/10.1016/j.wear.2013.04.010.

Gideon, B., Ward, L., Biddle, G. (2008). Duplex stainless steel welds and their susceptibility to intergranular corrosion. *J. Miner. Mater. Char. Eng.* 7 (3), 247-263. http://dx.doi.org/10.4236/jmmce.2008.73019.

Haghdadi, N., Cizek, P., Hodgson, P.D., Tari, V., Rohrer, G.S., Beladi, H. (2018). Effect of ferrite-to-austenite phase transformation path on the interface crystallographic character distributions in a duplex stainless steel. *Acta Mater.* 145, 196-209. https://doi.org/10.1016/j.actamat.2017.11.057.

Marcu Puscas, T., Molinari, A., Kazior, J., Pieczonka, T., Nykiel, M. (2001). Sintering transformations in mixtures of austenitic and ferritic stainless steel powders. *Powder Metall.* 44 (1), 48-52. https://doi.org/10.1179/003258901666167.

Mariappan, R., Kumar, P.K., Jayavelu, S., Dharmalingam, G., Prasad, M.A., Stalin, A. (2015). Wear properties of P/M duplex stainless steels developed from 316L and 430L powders. *Int. J. Chem. Tech. Res.* 8 (10), 109-115.

Mestra, A., Fargas, G., Anglada, M., Mateo, A. (2010). Sliding wear behavior of a duplex stainless steel. *Key Eng. Mater.* 423, 125-130. https://doi.org/10.4028/www.scientific.net/KEM.423.125.

Okayasu, M., Ishida, D. (2019). Effect of Microstructural Characteristics on Mechanical Properties of Austenitic, Ferritic, and γ-α Duplex Stainless Steels. *Metall. Mater. Trans. A* 50 (3), 1380-1388. https://doi.org/10.1007/s11661-018-5083-4.

Olsson, J.O., Groth, H.L. (1994). Evaporators made of solid duplex stainless steel. A new approach to reduced costs. *Desalination* 97 (1-3), 67-76. https://doi.org/10.1016/0011-9164(94)00075-1.

Olsson, J., Snis, M. (2007). Duplex—A new generation of stainless steels for desalination plants. *Desalination* 205 (1-3), 104-113. https://doi.org/10.1016/j.desal.2006.02.051.

Pohl, M., Storz, O., Glogowski, T. (2007). Effect of intermetallic precipitations on the properties of duplex stainless steel. *Mater. Charact.* 58 (1), 65-71. https://doi.org/10.1016/j.matchar.2006.03.015.

Raja Annamalai, A., Upadhyaya, A., Agrawal, D.K. (2015). Effect of heating mode and electrochemical response on austenitic and ferritic stainless steels. *Can. Metall. Q.* 54 (2), 142-148. https://doi.org/10.1179/1879139515Y.0000000001.

Xu, X., Wessman, S., Odqvist, J., King, S.M., Hedström, P. (2019). Nanostructure, microstructure and mechanical properties of duplex stainless steels 25Cr-7 Ni and 22Cr-5Ni (wt.%) aged at 325 °C. *Mater. Sci. Eng. A* 754, 512-520. https://doi.org/10.1016/j.msea.2019.03.046.